Research Article

Experimental and Numerical Study on the Vortical Flow of MULDICON Wing Configuration

Ibrahim Madan [iD],[1] **Jiun-Jih Miau** [iD],[1] **and Shabudin Bin Mat**[2]

[1]*Department of Aeronautics and Astronautics, National Cheng Kung University, Tainan 70101, Taiwan*
[2]*UTM Aerolab, Institute for Vehicle System & Engineering (IVeSE), Universiti Teknologi Malaysia, Johor, Malaysia 81310*

Correspondence should be addressed to Ibrahim Madan; engibrahimmadan5@gmail.com

This paper highlights the results and comparison of the flow topology investigation above the unmanned combat aerial vehicle (UCAV) configuration, namely, multidisciplinary design configuration (MULDICON), with modified leading-edge profile at the apex region from a sharp to a blunt profile to reduce the complexity of the flow structure above the wing. It was found from the flow visualization results that at a low angle of attack, for instance, 10°, the onset of the flow separation took place near the apex region; the onset of a tip vortex at the wing tip was also detected. At a medium angle of attack, for instance, 15°, the onset of the flow separation moved further upstream with the formation of the apex vortex, and the magnitude of the tip vortex increased due to increasing incoming flow with increasing the angle of attack. At higher angle of attack, for instance, 20°, the apex vortex intensity increased and wing tip vortices shedding is observed. Furthermore, at an angle of attack of 25°, the configuration is partially stalled, while a complete stalled occurred at an angle of attack of 30°. The current results obtained from this study have shown that the configuration has a maximum lift coefficient of 0.8 obtained from the K-Omega-SST turbulence model while it is 0.93 calculated from the Spalart-Allmaras turbulence model, while the maximum drag coefficient is 0.31 and 0.35, respectively, when calculated for the K-Omega-SST turbulence model and the Spalart-Allmaras turbulence model at an AOA of 25°. The flow visualization results revealed that there is a single flow separation due to modified leading edge from sharp to blunt, thus flow complexity is reduced.

1. Introduction

The design of unmanned combat aerial vehicles (UCAV) continues to be a major challenge among aeronautical engineers and researchers. In the recent studies several wing configurations were introduced such as the diamond configuration, stability and control configuration (SACCON), and multidisciplinary design configuration (MULDICON) in order to obtain optimum aerodynamic characteristics on the UCAV. In addition, the leading-edge profiles of these configurations are designed as sharp leading edge at the apex followed by a blunt leading edge at the midwing section where the bluntness is defined by the radius of the leading edge [1, 2]. The flow topology above a blunt leading-edge delta wing is very complicated and unresolved due to that the onset of the primary vortex is not fixed at the apex of

the configuration unlike the case of the sharp leading edge where the onset of the primary vortex is fixed at the apex of the configuration primary. Therefore, the vortex structure above these delta wing configurations is very complicated which led to several experimental and numerical studies to further understand the flow structure above these delta wing configurations stated above [2]. Furthermore, there are numerous ongoing UCAV programs in the Asia region at present such as in India Autonomous Unmanned Research Aircraft (AURA) and South Korea (K-X) UCAV where the main focus of these UCAV programs is on delta wing configurations with low to medium sweep angle, i.e., 35° to 55°, including different leading-edge profiles such as blunt and sharp leading edges, to improve performance, endurance, and to maximize the lift of the actual flight at a high angles of attack where the flow could be complicated above
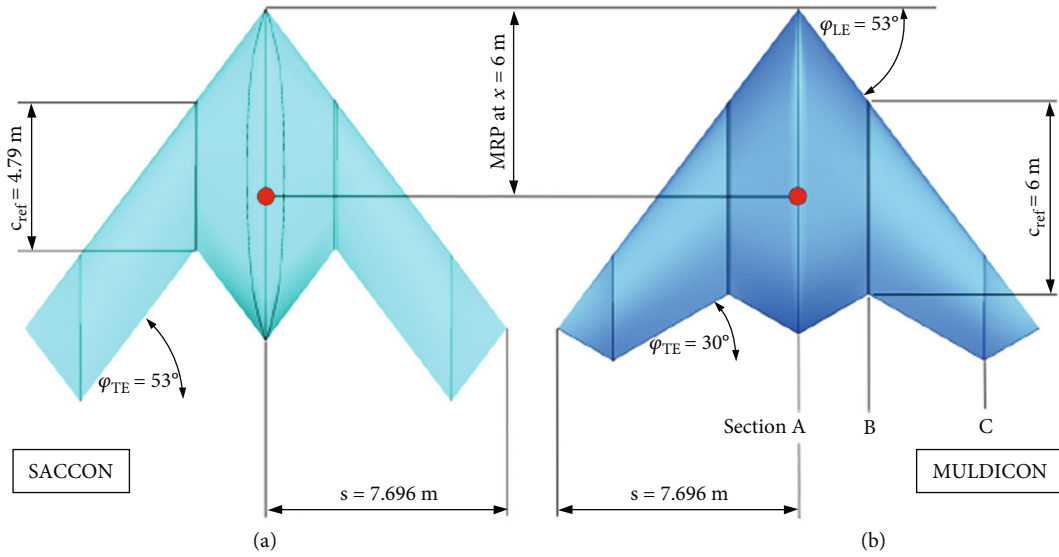
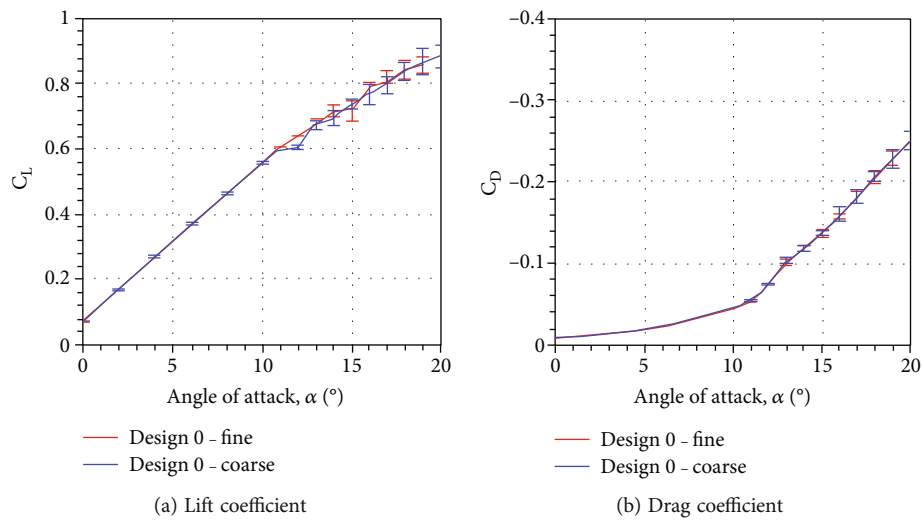Figure 1: Generic profile of SACCON (a) and MULDICON (b) [9, 10].

Figure 2: Comparison of lift and drag coefficients versus angle of attack [17].

the configuration due to the multiple flow separations [3]. Correspondingly, several designs and concepts involved with delta wing have been investigated including blended flying wing configurations to achieve a stealthy and agile attribute which are the major challenges for advanced UCAV design, and similarly-swept angle lambda wing configuration [4]. To point out, prior to the development of SACCON and MULDICON similar programs were conducted under The Applied Vehicle Technology (AVT) research program started with numerical and experimental investigations on the vortex topology of delta-wing configurations [4]. The program which started with a research team, namely, AVT-080, which focuses on the aerodynamics properties of a sharp leading-edge profile, followed by another research team, namely, AVT-113, to further investigate the vortex structure of blunt leading-edge profile [4]. Moreover, an additional research team, namely, AVT-161, has been commenced to concentrate on the assessment of

stability and control prediction methods for air and sea vehicles including a new configuration concept called the stability and control configuration (SACCON) to carry out numerical and experimental investigations on the stability and control of the SACCON [5]. Furthermore, the SACCON design is a lambda wing with a leading edge sweep angle of 53° and 5° twist at the wing tip to delay the stall at high angle of attack. It also comes with three main sections, namely, the fuselage, outer wing section, and wing tip with different leading-edge profiles starting from the apex towards the trailing edge. The current results illustrate that the flow over the SACCON is very complicated due to multiple leading-edge flow separations [5, 6]. In the same way, a research group under AVT program, namely, AVT-183, to investigate and predict the onset of the flow separation of the newly introduced configuration named DIAMOND wing which is simplified from SACCON design. The purpose of establishing such a research team is
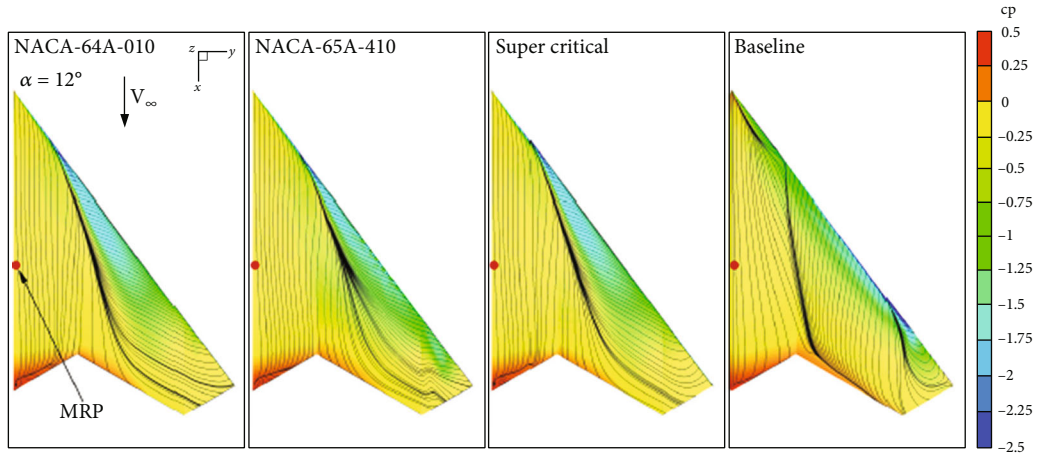
Figure 3: Pressure distribution and skin friction lines above MULDICON for four different airfoil profiles at an angle of attack of 12° [18].
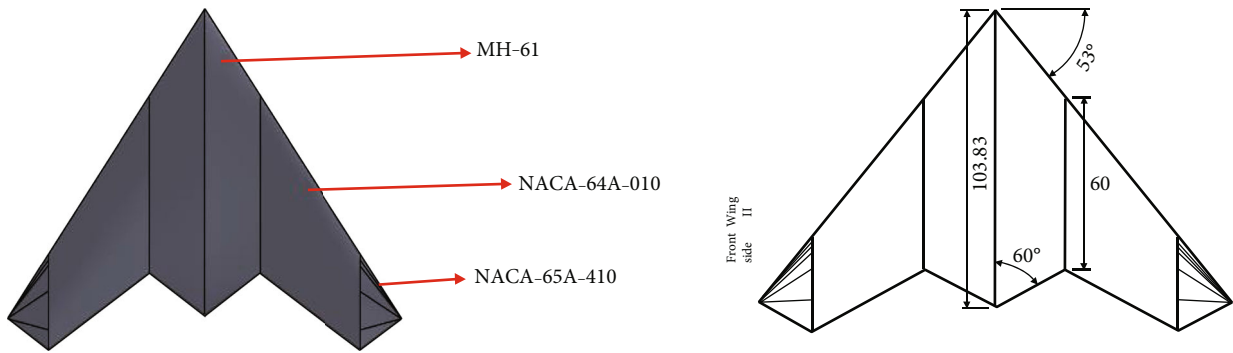

Figure 4: Modified MULDICON.

to emphasis on the onset and progression of the flow separation, particularly for a constant blunt leading edge of diamond-shaped configuration which comes with a 53° leading-edge sweep angle [7]. Lastly, a recently introduced configuration, namely, multidisciplinary design configuration (MULDICON), under a research team that is AVT-251 which is established to apply advanced numerical solutions and approaches to a UAV design for certain military missions. Additionally, the research team is divided into five subgroups which are the Design Specification and Assessment Group (DSAG), Aerodynamic Shaping Group (ASG), Engine Integration Group (EIG), Control Concepts Group (CCG), and Structural Concepts Group (SCG) [8]. Notably, the MULDICON was based on SACCON; however, a significant change from SACCON was that the trailing-edge sweep angle has been reduced from 53° to 30° in the MULDICON to reduce the load on the control surface devices and to increase the configuration area, thus increases lift force. Both configurations are shown in Figure 1 [9, 10].

To emphasize the flow topology of both sharp and blunt leading-edge profiles of the delta wing, the flow topology of the delta wing with sharp a leading edge is dominated by a conical-shape primary vortex above the wing with a fixed separation line at the leading edge where increasing the angle of attack results in increasing the magnitude of the primary vortex while its magnitude decreases as it travels

Table 1: MULDICON dimensions for numerical simulation.

Description	Value
Wingspan	0.154 m
Wing area	0.00803 m^2
Root chord	0.06 m
Tip chord	0.323 m
Sweep angle	53°

Table 2: MULDICON dimensions for experimental flow visualization.

Description	Value
Wingspan	0.25 m
Wing area	0.0212 m^2
Blockage ratio	5.10% at AOA = 30 ◦
Root chord	0.0975 m
Tip chord	0.05 cm
Sweep angle	53°

downstream towards the trailing edge. Correspondingly, a secondary vortex appears underneath the primary vortex due to the side strong flow towards the leading edge [11, 12].
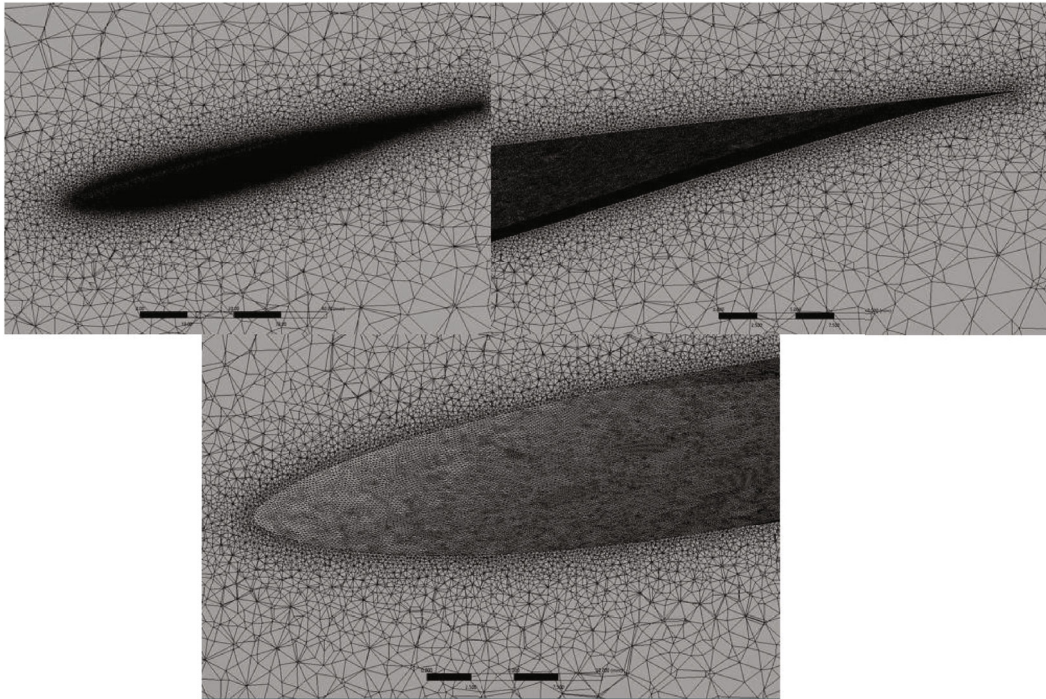
FIGURE 5: View of volume mesh of the configuration.

Meanwhile, the flow topology above blunt-edged delta wing is complicated due to leading edge bluntness where the onset of the flow separation is not fixed at the leading edge as the case of sharp leading profile, but the flow separation takes place somewhere near the apex of the wing. In detail, at low angle of attack the attached nonseparated flow is dominant, and the onset of the primary vortex takes place at a position downstream from the wing apex due to the small ratio between the leading radius and the wing span. The factors that affect the flow topology of a blunt leading profile are governed by Reynolds number, angle of attack, Mach number, and the bluntness ratio [13–16]. Moreover, in the effort of numerical studies and investigations of the flow topology above MULDI-CON, Aref et al. investigated the aerodynamic characteristic computationally with angle of attack range of 0° to 20°, and the results obtained show that the configuration has a linear aerodynamic regime up to an angle of attack of 16°. Furthermore, the lift coefficient captured at an angle of attack of 20° is 0.9, meanwhile the drag coefficient is 0.25 as indicated in Figure 2 [17]. Comparatively, Schutte and Vormweg studied the effect of different leading-edge profiles on the flow topology and the aerodynamic performance above MULDICON. The study objective is to investigate the flow topology on the three different leading-edge profiles, namely, NACA-64A-010 which is noncambered airfoil, NACA-65A-410 which is cambered airfoil, and supercritical airfoil which delays the onset of the wave drag, and compare the results of these three airfoils to the baseline configuration. The results obtained for the three stated airfoils indicate that the flow separations and complexity are reduced compared to the baseline configuration which has multiple flow separations as can be seen in Figure 3. The results obtained have also shown that these

critical airfoils and NACA-65A-410 airfoils can provide a high lift coefficient and a low drag coefficient [18].

The flow topology above MULDICON is complex which leads to multiple flow separations due to the current arrangement of three leading edge profiles starting from the apex towards the rear part of the configuration as the following: sharp, blunt, and sharp. The effort in this study tends to decrease the multiple flow separations by rearranging the leading-edge profiles from the current design to blunt and blunt and sharp profiles.

2. Setup and Methodology

2.1. Test Configuration. The chosen leading-edge profiles are arranged from the apex towards the rear part of the configuration as MH-61 airfoil with blunt leading-edge profile which is suitable for flying wing designs as it provides high lift and low drag with max camber of 1.4% at 37.3% chord with leading edge radius of 2.5 mm which defines its bluntness, NACA A64-010 noncambered airfoil to reduce the multiple separations occurred by the sharp leading profile of the original design was due to its leading edge bluntness which has 2.5 mm radius as well, and lastly NACA A65-410 which is cambered airfoil with Max camber of 2.2% at 50% chord with sharp leading edge profile to provide sufficient lift force at high angle of attack as the modified MULDICON can be seen in Figure 4. Furthermore, two models with different scale ratios were used for this study, the first model scaled down to a ratio of 1/100 for the numerical simulations as the dimensions are indicated in Table 1 with inlet velocity of 45 m/s which is corresponding to Reynolds number of 1.8×10^5, the second model scaled
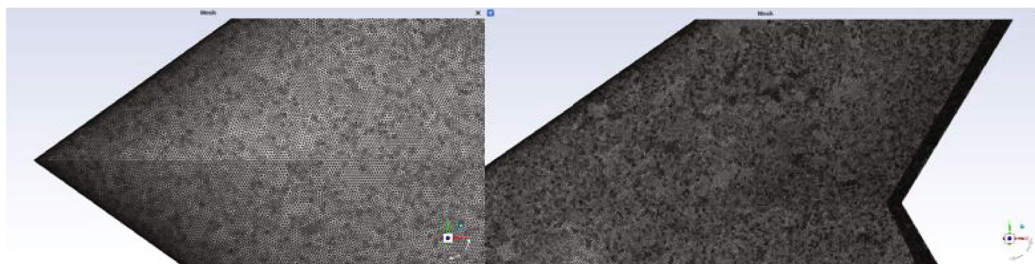
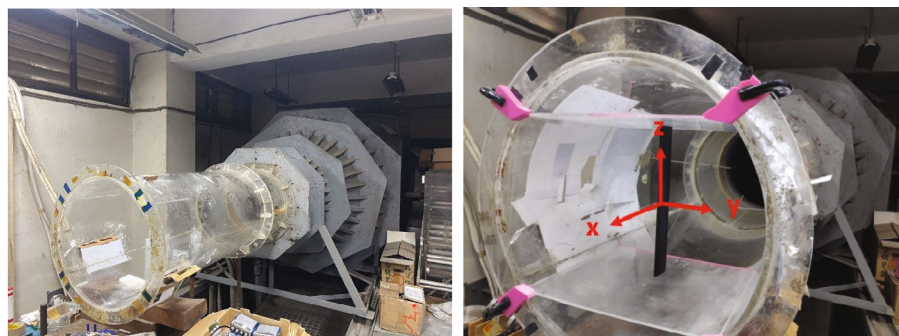Figure 6: View of surface mesh of the configuration.

Figure 7: The NCKU open-jet wind tunnel.

down to a ratio of 1/60 for the experimental study as the dimensions are illustrated in Table 2 with inlet velocity of 27.3 m/s which is corresponding to Reynolds number of 1.8×10^5 as well where the reason for larger model for the experimental work is for spreading the oil film and to place the tuft on the surface as well as better observation of the flow details above the configuration where the used surface tuft are 12 rows of 8 mm long canvas tuft and 5 mm gaps between each row. In addition, the experimental model constructed by using 3D printing technology and brushed with sandpapers several times to ensure smoothness.

2.2. Computational Grid. The grid used for the numerical simulation study was generated using the Ansys Fluent meshing tool, and the average number of elements for all cases is about 13 million including the volume mesh of the flow domain and the UCAV surface mesh where the UCAV surface mesh was set to hard meshing behavior to avoid any affection by the proximity and curvatures for the selected number of mesh elements with overall maximum skewness quality of 0.85 and minimum orthogonal quality of 0.15. Moreover, the volume mesh is completely unstructured with growing ratio of 1.2. The volume mesh and surface mesh are illustrated in Figures 5 and 6, respectively.

2.3. Fluent Setup. The Ansys software was used to solve the flow above the wing by calculating the N-S equation for three-dimensional flow under incompressible flow conditions. The flow domain has an inlet distance of 300 mm which is 5 times the UCAV root chord length of 60 mm with a velocity inlet of 45 m/s, and outlet distance of 600 mm which is 10 times the UCAV root chord length with a constant pressure outlet (static pressure) as the outlet boundary

Figure 8: The Model installation in NCKU wind tunnel at angle of attack of 15°.

condition. Moreover, the turbulence models used for this study are Spalart-Allmaras and K-Omega-SST as recommended by Ansys manual and discussed by [8] to evaluate the prediction of the turbulence effect and the aerodynamic coefficients of both turbulence models and to be compared with the baseline configuration results. Additionally, a coupled second-order discretization was used where K is the kinetic energy of turbulence and the number of iterations is 750 to ensure convergence of the solution.

2.4. Mesh Independence Study. In order to ensure mesh accuracy a mesh independence study was carried out in three steps. The first step has around 6 million elements to ensure
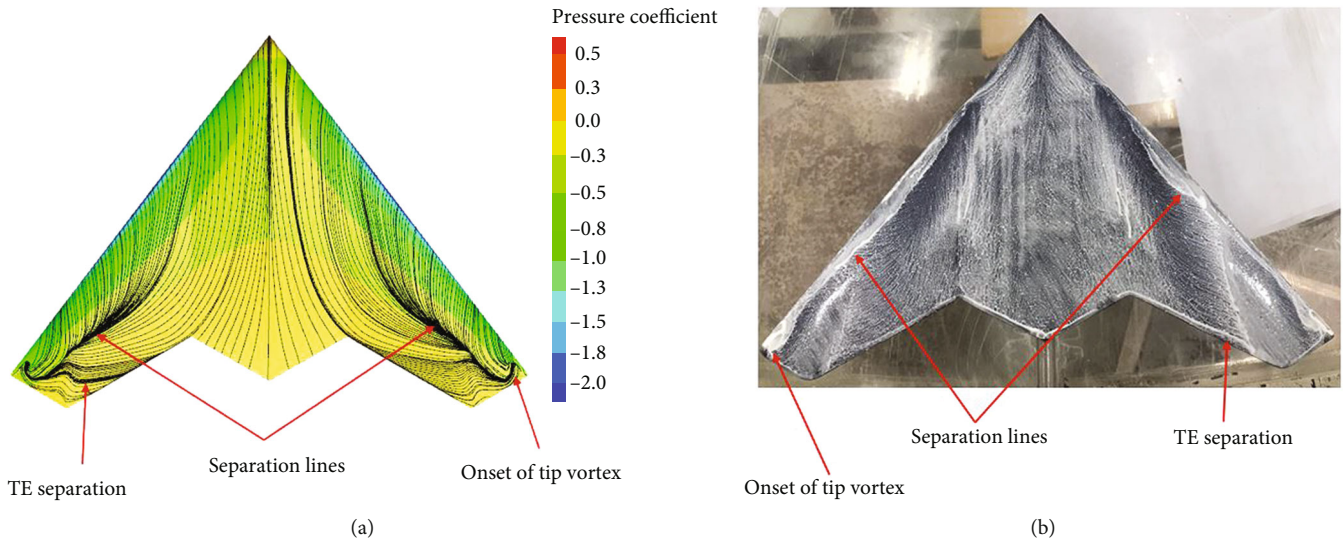
FIGURE 9: CFD K-Omega-SST result (a) compared to oil film results (b); AOA = 10∘, Re = 1.8×10^5.

convergence of residual error to 10^{-4}, while the second step has around 9 million with 1.5 times increment to the number of elements in the first step. Lastly, the third step follows the same order as the second step and has around 13 million elements with an insignificant change in the results compared to the second step.

2.5. NCKU Wind Tunnel Facility. The experiments were conducted in the National Cheng Kung University (NCKU) open-jet wind tunnel which is featured with a circular test section of 0.5 m in diameter, as can be seen in Figure 7, and a maximum velocity of 30 m/s. The freestream turbulence intensity is less than 0.6% at the maximum velocity of the wind tunnel, and the model installation in the wind tunnel is illustrated in Figure 8.

3. Results and Discussion

A comparison of the numerical analysis and wind-tunnel experiments obtained results on the MULDICON at National Cheng Kung University NCKU for $\alpha = 10∘$, 15°, 20°, 25°, and 30° at Re = 1.8×10^5 are illustrated in the figures, respectively, where Re is based on the incoming freestream velocity, the root chord length of the model, and angle of attack. As can be seen from the experimental oil-film visualization results which obtained under the five angles of attack that there is one flow separation at the leading edge due to the modified leading-edge profiles from sharp to blunt; thus flow complexity is reduced compared to the baseline which has two flow separations one at the apex due to the sharp leading-edge profile and the second separation at the wing leading edge due to the blunt leading-edge profile. Furthermore, the flow separation is not initiated at the apex of the wing where the onset of the flow separation took place at a position near the apex which is apparently due to the leading-edge bluntness as discussed by [13–16, 19]. To further emphasize the flow mechanism, at a low angle of attack, for instance, 10°, the flow field is dom-

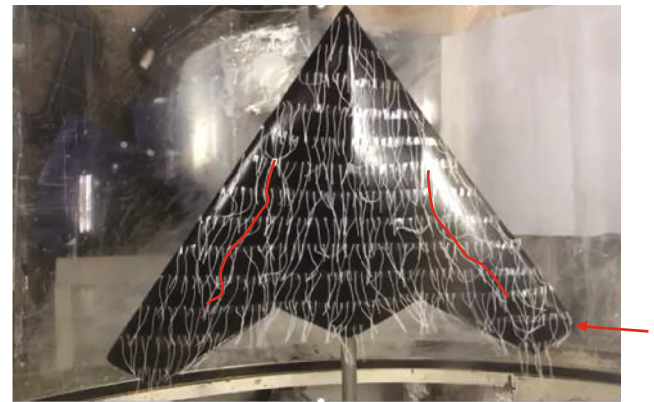FIGURE 10: Surface tuft method result at AOA = 10∘ and Re = 1.8×10^5.

inated by a large region of attached flow. The onset of the tip vortex at the wing tip is initiated due to the sharp leading edge profile, while the onset of the flow separation took place near the apex as the separation lines can be seen inboard of the configuration from the skin friction lines in the pressure contour of the numerical results and the oil-film footprint of the experimental results, as indicated in Figure 9. In addition, the separation lines of the oil-film experimental results are shown slightly outboard compared to the numerical solution due to that the numerical calculations are not capable of unveiling the exact detailed flow structures revealed by the oil-film visualization method which requires improvement to the numerical method, especially in those areas where flow separations and flow re-attachments could occur.

A surface tuft method was carried out in the effort of obtaining a 3D picture of the vortex structure above the configuration. The results obtained illustrate that the onset of the tip vortex is noticed by the bending trend of the tuft on both sides of the configuration which follows the flow direction as indicated by the red arrow shown in Figure 10.
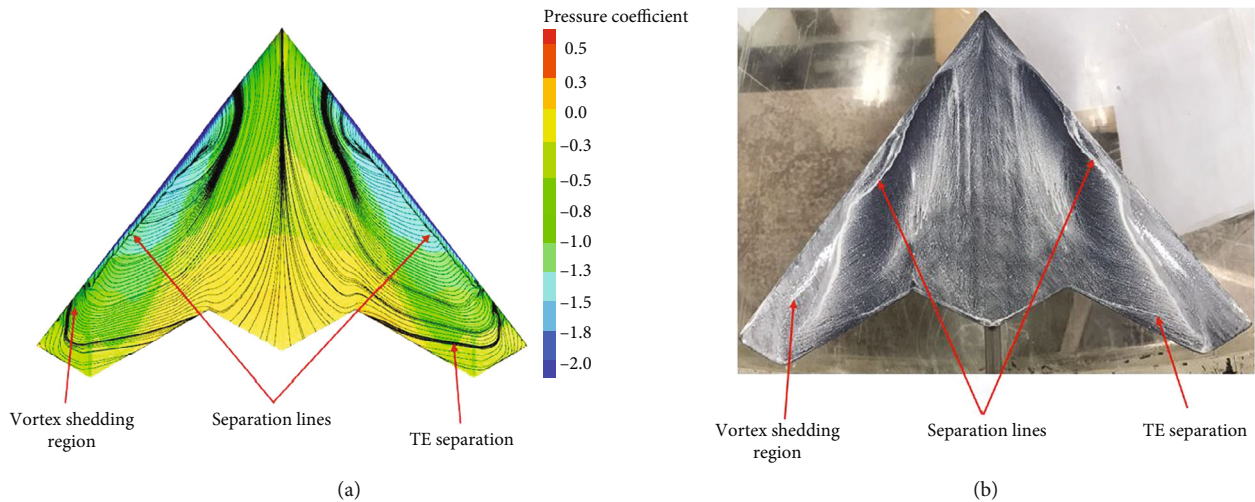
(a)

(b)

FIGURE 11: CFD K-Omega-SST result (a) compared to oil film results (b); AOA = 15∘ and Re = 1.8×10^5.

Additionally, the flow separation region near the leading edge has been identified and traced with the red line, while near the apex and midsection of the configuration is dominated by a large region of attached flow which is similar to the trend in the CFD results.

Similarly, a further increase in the angle of attack, for instance, 15°, shifts the onset of the leading-edge separation further upstream towards the apex of the wing due to increasing the flow velocity over the wing. The oil-film results clearly show the locations of the flow separation lines and the inboard shift with an enlarged region of the tip vortex due to the apex vortex which increases the spanwise flow near the tips and results in increasing its intensity as well. Furthermore, multiple leading-edge separations are easily observed compared to the previous case, as illustrated in Figure 11. Additionally, the surface tuft method result as well indicates that the region of the spanwise flow at the wing tip is enlarged due to the increment of alpha, while the footprint of the tuft at the leading edge indicates the upward shift of the flow separation line, as can be seen in Figure 12.

Further increase in the angle of attack, for instance, 20°, the onset of the flow separation at the leading edge can be clearly identified from the numerical and experimental results as shown in Figure 13 which is noted further upstream near the apex where the apex vortex is smaller in radius compared to the results of low to medium angles of attack. Additionally, the small radius of the apex vortex indicates increasing its suction magnitude and that explains the vortices shedding from a location near the wing tip towards upstream while the spanwise flow intensity at the wing tip is less due to the wider wing tip separation. Moreover, the oil-film result indicates a similar trend of the flow separation onset near the apex as unveiled by the numerical result and also indicates the vortex shedding region where the upstream shedding of the vortices of the delta wing is discussed by [20].

The oil film experiment does not provide a 3D picture of such vortices shedding which required a surface tuft method
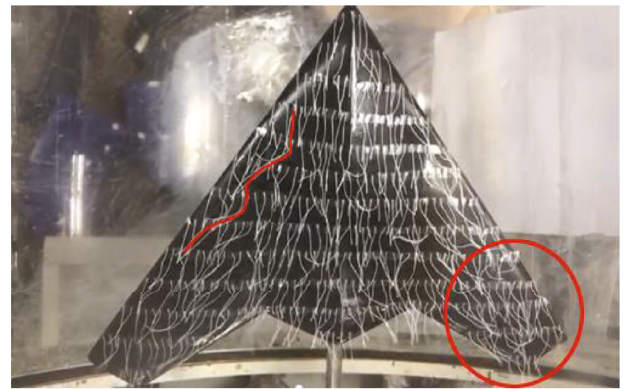

FIGURE 12: Surface tuft method result at AOA = 15∘ and Re = 1.8×10^5.

experiment to obtain a 3D picture of the vortices shedding from a location near the wing tip towards upstream. As can be seen from Figure 14, the vortices shedding is clearly identified (spanwise flow), as indicated by the large red circle on the right-side wing tip where the spanwise flow region increases as well due to the wide flow separation at the wing tip. Furthermore, increasing the angle of attack moves the onset of the flow separation further upstream towards the apex as the location of the flow separation onset indicated by the small red circle at the top left side of the configuration where the upstream progression of the separation onset with increasing the angle of attack is discussed by [13–16].

Similarly, at an angle of attack of 25°, the onset of the flow separation moves further upstream towards the apex of the configuration. To be noticed at this stage is that the vortices shedding from the wing tip towards the apex become weaker as the spanwise flow along the leading edge is reduced which explains that the intensity of the apex vortex is insignificant, as illustrated in Figure 15 which also explains the poor increment of the lift coefficient compared to the previous cases, as notified in Figure 16. Furthermore,
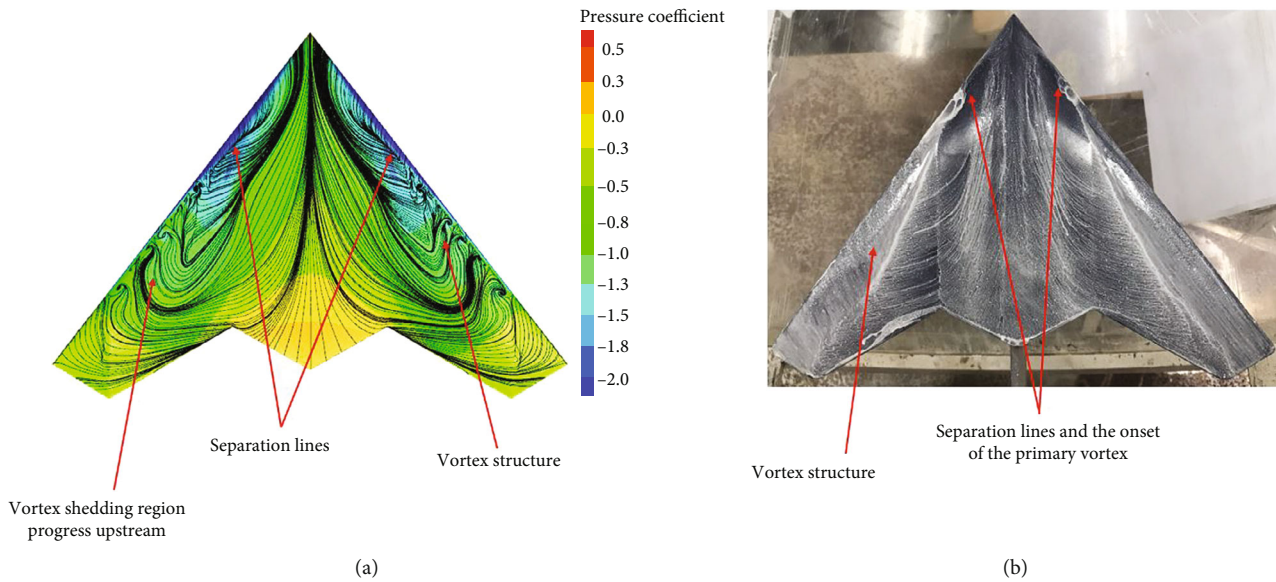
(a)

(b)

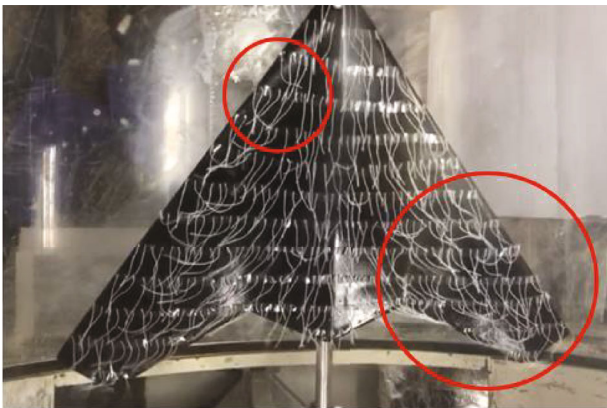FIGURE 13: CFD K-Omega-SST result (a) compared to oil film results (b); AOA = 20 ∘ and Re = 1.8×10^5.

FIGURE 14: Surface tuft method result at AOA = 20 ∘ and Re = 1.8×10^5.

Figure 15 shows an unsteady flow structure covering a large portion of the configuration which indicates that the configuration is partially stalled, especially at the wing tip and the midsection wing.

At an angle of attack of 30°, fully separated flow and unsteady flow structure are indicated at this stage, as illustrated in Figure 17. Multiple trailing edge separations and spiral separation at the midposition of each wing are marked with red circles which explains the descending lift coefficient and rapid increment of drag coefficient notified in Figure 16 which are associated with configuration complete stall condition. To be notified, the results of the surface tuft experiment were not included for both angles of attack of 25° and 30° due to the unsteady aerodynamics above the configuration which results in unsteady movement of the tuft and led to a lack of clear vision indicating partial and complete stall of the configuration at AOA 25° and at AOA 30°, respectively.

Figure 16 shows lift and drag coefficients trend verse angle of attack where the maximum lift coefficient of 0.8 is achieved for the K-Omega-SST turbulence model at an angle of attack of 25°, while the maximum lift coefficient of the Spalart-Allmaras turbulence model is 0.93 at the same angle of attack where beyond this the lift coefficient started to drop. In addition, the new MH-61 airfoil with a blunt leading-edge profile maintained a sufficient lift coefficient at a high angle of attack. On the other hand, the drag coefficient captured at an angle of attack of 25° is 0.31 for the K-Omega-SST turbulence model and 0.35 for Spalart-Allmaras turbulence model where beyond that, the drag coefficient increases rapidly due to the stall condition. A comparison of the baseline lift and drag coefficient has been included which indicates that the baseline configuration has a higher lift coefficient compared to the modified configuration of this study, and that is due to the bluntness of the leading edge, as blunt leading edge produces a smaller weak vortex structure compared to the sharp leading edge of the baseline configuration. In addition, lift and drag experimental data are not provided in this paper due to limitations of the experimental equipment, and the numerical lift and drag coefficients are provided as supplementary data where the main focus in this paper is on the flow visualization to ensure reduction of the flow complexity above the modified configuration.

Correspondingly, a comparison of the Cl/Cd ratio of the modified configuration for both turbulence models is illustrated in Figure 18 and compared to the baseline configuration. As can be seen, at low and moderate angles of attack, the baseline configuration has a higher Cl/Cd ratio compared to the modified configuration. Due to that, the baseline configuration has a higher lift coefficient as the vortex structures above the sharp leading edge are bigger and stronger compared to blunt leading-edge profiles.
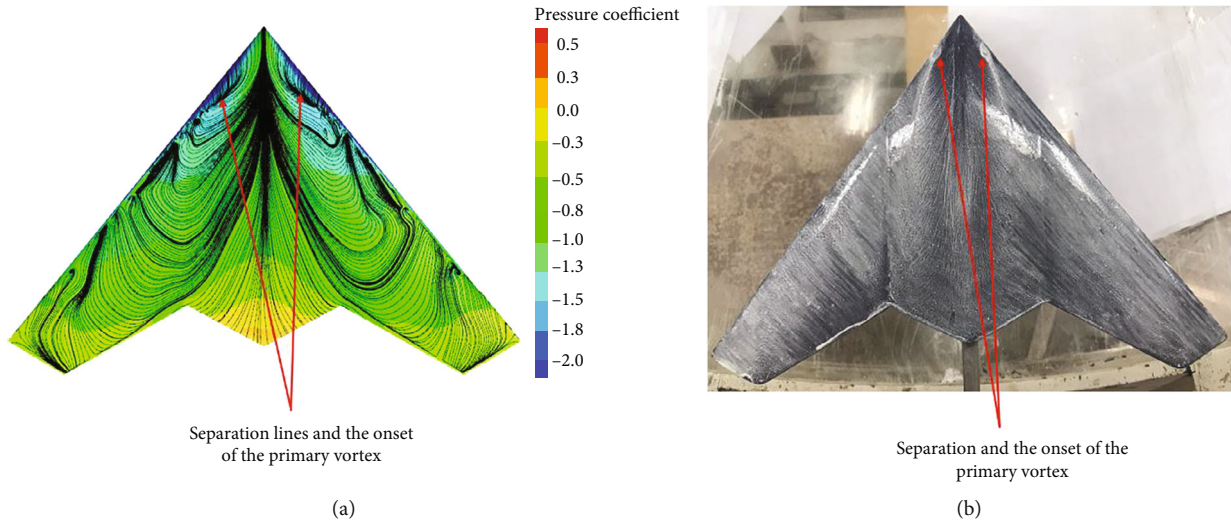
Separation lines and the onset
of the primary vortex

(a)

Separation and the onset of the
primary vortex

(b)

FIGURE 15: CFD K-Omega-SST result (a) compared to oil film results (b), AOA $=25°$, Re $=1.8 \times 10^5$.
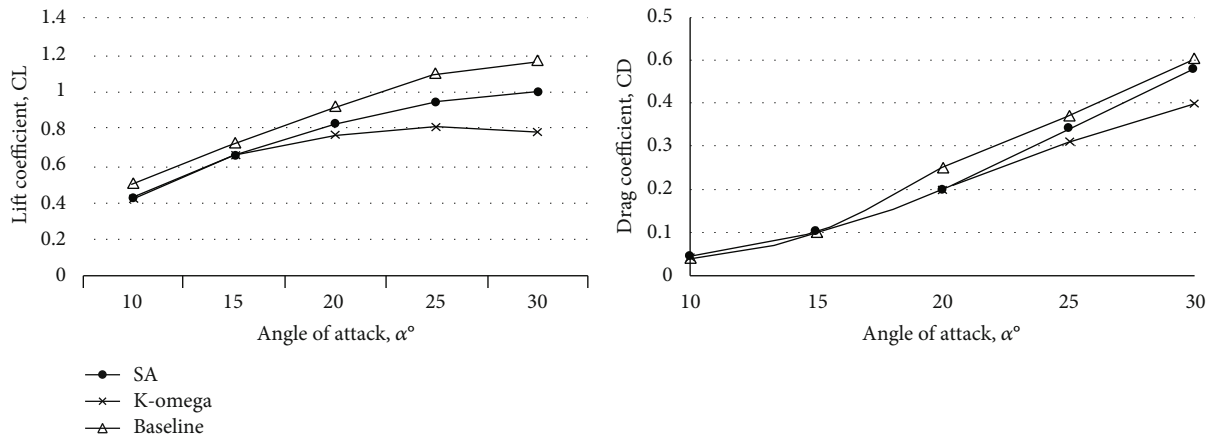

- SA
- K-omega
- Baseline

FIGURE 16: Lift and drag coefficients versus AOA obtained from the numerical analysis of MULDICON compared with baseline design aerodynamic performance results as discussed in [8].

Separation and the onset of the
primary vortex

TE separations

(a)

Separation and the onset of the
primary vortex

(b)

FIGURE 17: CFD K-Omega-SST result (a) compared to oil film results (b); AOA $= 30°$ and Re $= 1.8 \times 10^5$.

FIGURE 18: Lift and drag coefficient ratio versus AOA obtained from the numerical analysis of MULDICON compared with Baseline design aerodynamic performance results as discussed in [8].

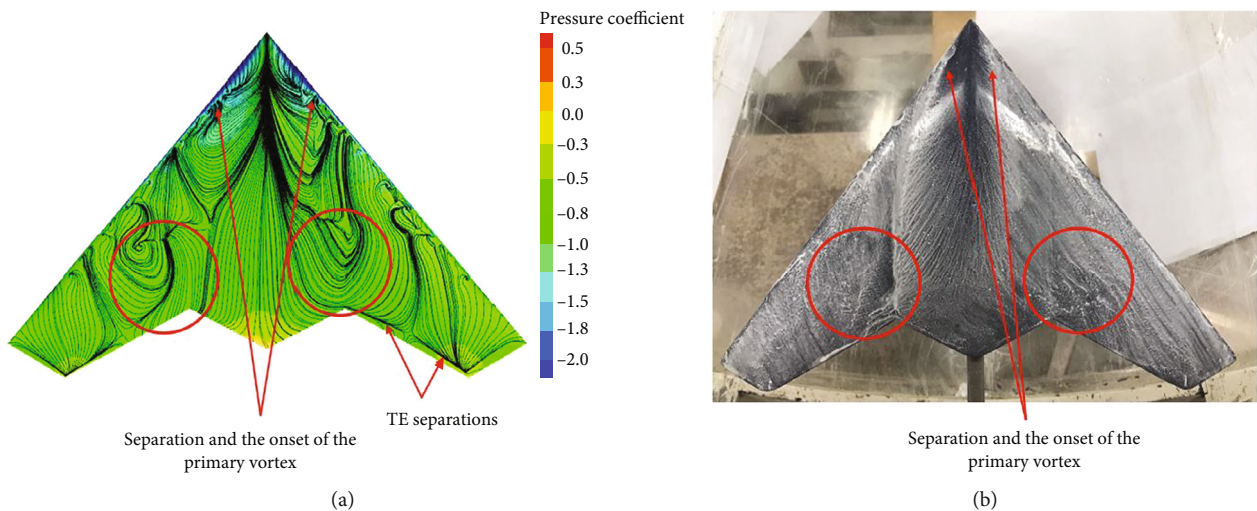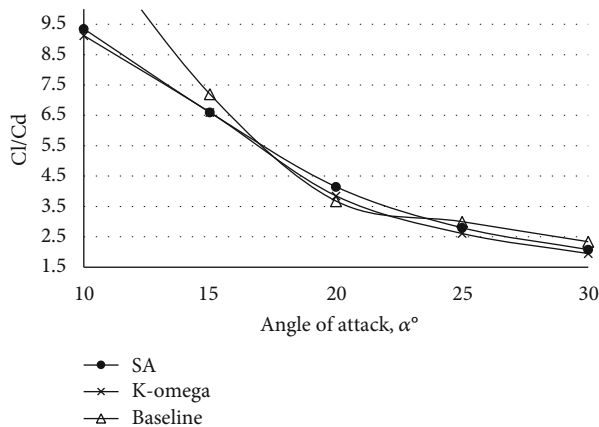## 4. Conclusions

In a numerical and experimental investigation study carried out at National Cheng Kung University (NCKU) of modified MULDICON UCAV. The results obtained from the numerical simulations show that the modified configuration with blunt leading-edge profile maintained a sufficient lift and low drag coefficient at high angle of attack where the lift coefficient of the K-Omega-SST turbulence model is 0.8, while for the Spalart-Allmaras turbulence model is 0.93. The flow visualization results unveiled that there is one flow separation due to modified leading edge from sharp to blunt, thus flow complexity is reduced compared to the baseline. Furthermore, at a low angle of attack, for instance, 10°, the onset of the flow separation took place at a location downstream of the apex, and an indication of the onset of the tip vortex is noticed due to the sharp leading-edge profile at the tip, while the attached flow is still dominant at this stage. Further increase in the angle of attack, for instance, 15°, the leading-edge flow separation is obvious, and the onset of the separation shifts further upstream towards the apex; at this stage, the apex vortex is identified as well. In addition, at a high angle of attack, for instance, 20°, the intensity of the apex vortex increases due to increasing incoming flow as well as wing tip vortices shedding upstream is noticed. At an angle of attack of 25°, the configuration is partially stalled, while it is completely stalled at an angle of attack of 30°.

Data Availability

The authors confirm that the data supporting the findings of this study are available within the article.

Conflicts of Interest

The authors declare that they have no conflicts of interest.

References

[1] D. Zimper and D. Hummel, "Analysis of the transonic flow around a unmanned combat aerial vehicle configuration," *Journal of Aircraft*, vol. 55, no. 2, pp. 571–586, 2018.

[2] J. M. Luckring, "A survey of factors affecting blunt-leading-edge separation for swept and semi-slender wings," in *28th AIAA Applied Aerodynamics Conference*, p. 4820, Chicago, IL, USA, 2010.

[3] J. M. Luckring and D. Hummel, *Chapter 24–What Was Learned from the New VFE-2 Experiments*, RTO-TR-AVT-113, 2008.

[4] J. M. Luckring, "Initial experiments and analysis of blunt-edge vortex flows for VFE-2 configurations at NASA Langley, USA," *Aerospace Science and Technology*, vol. 24, no. 1, pp. 10–21, 2013.

[5] R. M. Cummings and A. Schütte, "Integrated computational/ experimental approach to unmanned combat air vehicle stability and control estimation," *Journal of Aircraft*, vol. 49, no. 6, pp. 1542–1557, 2012.

[6] K. Huber, A. Schutte, and M. Rein, "Numerical investigation of the aerodynamic properties of a flying wing configuration," in *30th AIAA Applied Aerodynamics Conference*, p. 3325, New Orleans, LA, USA, 2012.

[7] J. M. Luckring and O. J. Boelens, "A reduced-complexity investigation of blunt leading-edge separation motivated by UCAV aerodynamics," in *53rd AIAA Aerospace Sciences Meeting*, p. 0061, Kissimmee, FL, USA, 2015.

[8] R. Nangia, M. Ghoreyshi, M. P. C. Van Rooij, and R. M. Cummings, "Aerodynamic design assessment and comparisons of the MULDICON UCAV concept," *Aerospace Science and Technology*, vol. 93, article 105321, 2019.

[9] A. Schütte, D. Hummel, and S. M. Hitzel, "Flow physics analyses of a generic unmanned combat aerial vehicle configuration," *Journal of Aircraft*, vol. 49, no. 6, pp. 1638–1651, 2012.

[10] R. M. Cummings, C. Liersch, and A. Schuette, "Multi-disciplinary design and performance assessment of effective, agile NATO air vehicles," in *2018 Applied Aerodynamics Conference*, p. 2838, Atlanta, GA, USA, 2018.

[11] M. Gad-el-Hak and R. F. Blackwelder, "The discrete vortices from a delta wing," *AIAA Journal*, vol. 23, no. 6, pp. 961-962, 1985.

[12] J. M. Luckring and O. J. Boelens, "A unit-problem investigation of blunt leading-edge separation motivated by AVT-161 SACCON research," in *NATO RTO Specialists Meeting AVT-189, no. NF1676L-12101*, 2011.

[13] A. Schütte, "Numerical investigations of vortical flow on swept wings with round leading edges," *Journal of Aircraft*, vol. 54, no. 2, pp. 572–601, 2017.

[14] A. Hövelmann, F. Knoth, and C. Breitsamter, "AVT-183 diamond wing flow field characteristics part 1: varying leading-

edge roughness and the effects on flow separation onset," *Aerospace Science and Technology*, vol. 57, pp. 18–30, 2016.

[15] I. Madan, N. Tajudin, M. Said et al., "Influence of active flow control on blunt-edged VFE-2 delta wing model," *International Journal of Automotive and Mechanical Engineering*, vol. 18, no. 1, pp. 8411–8422, 2021.

[16] S. Pfnür and C. Breitsamter, "Unsteady aerodynamics of a diamond wing configuration," *CEAS Aeronautical Journal*, vol. 9, no. 1, pp. 93–112, 2018.

[17] P. Aref, S. T. McGlone, J. Allen, M. Ghoreyshi, A. Jirasek, and A. J. Lofthouse, "Preliminary computational aerodynamic investigation of the NATO AVT-251 multi-disciplinary configuration," in *35th AIAA Applied Aerodynamics Conference*, p. 3412, Denver, CO, USA, 2017.

[18] A. Schütte, J. Vormweg, R. G. Maye, and T. Jeans, "Aerodynamic shaping design and vortical flow design aspects of a 53deg swept flying wing configuration," in *2018 Applied Aerodynamics Conference*, p. 2841, Atlanta, GA, USA, 2018.

[19] J. M. Luckring, *Chapter 4- Experimental Investigation of the Flow about a 65° Delta Wing in the NASA Langley National Transonic Facility*, NASA Langley Research Center, Hampton, VA, USA, 2014.

[20] J. J. Miau, W. H. Liu, and J. H. Chou, *Visualizations of Flow over a 50-Degree Sweep Delta Wing*, American Society of Mechanical Engineers, Fluids Engineering Division (Publication) FED, 1996.